THE JOURNAL OF PHYSICAL CHEMISTRY B

ARTICLE

pubs.acs.org/JPCB

UV-Absorption Spectra of Melanosomes Containing Varying 5,6-Dihydroxyindole and 5,6-Dihydroxyindole-2-Carboxylic Acid Content

Dana N. Peles[†] and John D. Simon[†,‡,*]

[†]Department of Chemistry, Duke University, Durham, North Carolina 27708, United States

[‡]Department of Chemistry, University of Virginia, Charlottesville, Virginia 22904, United States

ABSTRACT: Central to understanding the photochemical properties of melanosomes is a direct measurement of their absorption coefficients. Herein, the absorption spectra of intact melanosomes of varying molecular compositions and embryonic origins were measured and compared over the spectral range from 245 to 310 nm. The absorption spectra of melanosomes predominately comprised of the eumelanin pigment were found to differ significantly from their constituent precursor molecules, 5,6-dihydroxyindole (DHI) and 5,6-dihydroxyindole-2-carboxylic acid (DHICA). This difference was most notable in the UV-A region and indicates that the electronic structures of the monomeric building blocks, DHICA in particular, are significantly modified upon polymerization to the melanin pigment. Furthermore, in comparing embryonic differences, the absorption coefficients of melanosomes isolated from bovine retinal pigment epithelial (RPE) cells (originating from the primitive forebrain) were greater than those for bovine choroid or iris melanosomes (originating from the neural crest). This difference suggests that either the pigment is present in greater density in RPE melanosomes or that there is an underlying difference in molecular structure.

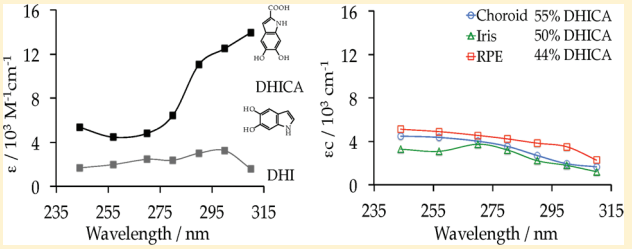

INTRODUCTION

Melanosomes are naturally occurring biological pigment assemblies predominately comprised of melanin. Melanin is categorized by two distinct classes, pheomelanin (red) and eumelanin (black). Although these two classes of melanin share a common origin to their biosynthesis, they are differentiated by specific molecular reactions occurring early in pigment production. Pure eumelanin can be found in nature, thereby enabling the study of its chemical properties. Pheomelanin is largely present in mixtures with eumelanin, and this renders it difficult to elucidate the intrinsic properties of this class of pigments using natural sources.

Detailed chemical studies demonstrate that eumelanin is a heterogeneous macromolecule derived from copolymerization of two molecular precursors, 5,6-dihydroxyindole (DHI) and 5,6-dihydroxyindole-2-carboxylic acid (DHICA).[1−3] Many functions have been attributed to eumelanin, but it is the role of photoprotection that is often the most cited.[4−6] Central to understanding the relationship between melanin and photoprotection is the need to have a quantitative measurement of the absorption spectra of intact melanosomes.

In quantifying the absorption properties of melanosomes, it is important to understand that the lack of knowledge about the molecular structure of the melanin means that the absorption coefficients are reported as the product εc, in units of inverse length. The optical properties of intact melanosomes have been determined through indirect measurements that require assumptions about the thermodynamic properties of the organelles.[14−19] For example, Jacques et al. utilized the indirect technique of explosive vaporization to calculate internal absorption coefficients of several types of melanosomes.[14,15] In this method, the absorption coefficient is deduced from assumed thermodynamic properties of the melanosome and the threshold temperature measured after heating with a pulsed laser in situ. While most of this work was focused in the midvisible wavelength range, a general wavelength-dependent absorption coefficient was predicted based on the scaling of an in vivo spectrophotometer measurement of cutaneous melanin to the acquired data,[14,15] giving a wavelength-dependent absorption coefficient for cutaneous melanosomes of $\varepsilon c(\lambda_{nm}) = 1.70 \times 10^{12}\ \lambda^{-3.48}\ cm^{-1}$. The quantity $\varepsilon c(\lambda_{nm})$ for retinal pigment epithelium (RPE) melanosomes was predicted to show the same wavelength dependence but to be greater in magnitude by a factor of ~3.8.

Despite this considerable effort to determine the absorption coefficient of melanosomes, it remains to be established that the values determined actually reflect the absorption coefficient of an intact, natural melanosome. Melanosomes predominately comprised of eumelanin are contained in several tissues of the eye: choroid, iris, and RPE.[7−9] These cells are also of differing embryonic origin: RPE cells are derived from the outer neuroectodermal sheath of the eyecup and the iris and choroid melanocytes, the cells that synthesize the melanosomes, originate from the neural crest, which is the same embryonic origin as cutaneous (skin) melanocytes.[10−13] Studies of the eumelanin isolated from these different tissues in bovine eyes display a range of DHICA:DHI

Received: June 27, 2011
Revised: September 7, 2011
Published: September 19, 2011

monomer ratios.[8] In addition, these ratios differ for the same melanosome (e.g., iris) isolated from newborn and adult bovine eyes. Thus, the bovine eye provides a unique system for examining how the absorption coefficients of melanosomes vary for differing molecular composition and embryonic origin, and such studies could ultimately provide insight into the macroscopic biological function of photoprotection.

We recently demonstrated that photoemission electron microscope (PEEM) images of intact melanosomes on a photoemissive substrate can be used to determine the absorption coefficients of individual melanosomes,[20−22] and have determined the absorption coefficient at λ = 244 nm for melanosomes of varying DHICA:DHI ratios.[21] Those single wavelength results suggested the absorption coefficient increases with increasing DHICA content. In an effort to further examine whether the εc of these melanosomes is well characterized by an additive relationship of the absorption properties of DHI and DHICA in the UV region, we have acquired the absorption spectrum of single melanosomes from λ = 244 to 310 nm. We find that the absorption spectrum of the melanosomes cannot be modeled in terms of the sum of the absorption properties of the constituent monomers. In addition, the data deviate from the previous report by Jacques,[14,15] and within error, a single function $\varepsilon c(\lambda_{nm})$ can be used to model the data.

MATERIALS AND METHODS

Sample Isolation and Preparation. Details regarding the isolation of the melanosomes used from bovine RPE, iris and choroid have been previously published along with their chemical and structural analyses.[8] Briefly, bovine eyes were hemisected at the equator using stainless scalpel and scissors to cut through the sclera, and the eye was separated into the anterior and posterior eyecups. From the anterior segment, the iris and cilliary body were isolated. From the posterior segment, the neural retina was gently lifted and removed to expose the RPE monolayer. RPE cells were isolated by gentle scraping with a scalpel. After the removal of RPE cells, the choroid membrane was lifted and separated from the nonpigmented sclera. RPE cells were homogenized and the melanosomes were purified using a sucrose gradient. The iris and choroid were processed in parallel, and the melanosomes were extracted from the tissue through enzymatic degradation.

Photoemission Electron Microscopy. Details of the Elmitec ultrahigh vacuum PEEM have been previously described in detail.[23] Substrates were prepared from a wafer of n-type 4*H*-SiC, purchased from Cree, Inc. (Durham, NC). The wafer was further chemomechanically polished by NOVASIC (Le Bourget-du-Lac, France) and cleaved to square regions of 1 cm^2 by American Precision Dicing, Inc. (San Jose, CA). Individual substrates were then subjected to a simple solvent cleaning process: substrates were placed in subsequent baths of trichloroethylene, acetone, and methanol for 5 min each and then dried under a steady flow of nitrogen gas. Immediately prior to experimentation, isolated melanosomes were suspended in a Nanopure water solution and deposited on the substrate in 0.5 μL aliquots. The samples were air-dried (<30 min) with minimal exposure to ultraviolet light and subsequently transferred under ultrahigh vacuum into the PEEM chamber for data collection. To ensure a large sampling, melanosomes were imaged at fields of view of 150 μm.

An intracavity doubled Ar^+ ion continuous wave (CW) laser was initially used to illuminate the sample at λ = 244 nm for purposes of finding and focusing the sample prior to wavelength scans with the tunable laser source. Laser excitation utilized for the wavelength dependent absorption experiments was provided by a solid-state tunable nanosecond laser system from Opotek, Inc. (Carlsbad, CA) at an angle of incidence of approximately 77° from the surface normal. Data was collected at the following wavelengths: 244 nm (5.08 eV), 257 nm (4.82 eV), 270 nm (4.59 eV), 280 nm (4.43 eV), 290 nm (4.28 eV), 300 nm (4.13 eV), and 310 nm (4.00 eV). The polarization of the light was parallel to the plane of incidence. To avoid noted space-charge effects[24] and physical disruption of the melanosomes[25] resulting from pulsed laser sources, a neutral density filter was inserted in the beam path to reduce the average laser power. The maximum pulse energy, after the neutral density filter, was at most 12 mJ/cm^2 for λ = 244 nm and decreased at longer wavelengths. This maximum pulse energy is less than 10% of the previously calculated photodisruption threshold of 153.6 mJ/cm^2.[25] At each wavelength, laser power and optical alignment were optimized prior to acquisition of the digital image. All images were captured with a cooled DVC-1500 M digital camera from DVC Company, Inc. (Austin, TX) with a resolution of 1392 × 1040 pixels × 12 bits. As a result of varied laser power across wavelengths, the acquisition times were 5, 7, 14, 28, 42, 50, and 50 min for λ = 244, 257, 270, 280, 290, 300, and 310 nm, respectively.

Determination of the Absorption Coefficient from the PEEM Image. Details regarding the calculation of the absorption coefficient, εc, from the PEEM image have been previously published.[20,21] Briefly, εc was calculated with the Beer−Lambert law

$$\varepsilon c = Al^{-1} = l^{-1}\log(I_0/I) \quad (1)$$

after values were obtained for the path length, l, and the incident and transmitted intensities of light, I_0 and I, respectively. Averages of the photoemission current of the portion of unobstructed substrate surrounding the shadow provided values for I_0, whereas averages of the photoemission current of the shadow region immediately behind the melanosomes provided corresponding values for I. In the PEEM images, a Fraunhofer diffraction pattern is observed in the shadow region of the melanosomes. As has been previously discussed,[20,26] it is the portion of the shadow that lies inside the calculated first diffraction ring that is void of significant scattering effects and thus it was this region that was used to calculate the average photoemission current of the shadow. The calculated distance from the center of the melanosome that defines this region is expressed by

$$d = \left(\frac{\lambda m_0 2b}{\pi 2a\varepsilon \tan(\alpha)}\right) \quad (2)$$

where α = 13°, m_0 = 3.83166, λ is the wavelength, a and b are the lengths of the major and minor ellipsoidal radii of the melanosome, and ε is the ellipsoidal axial ratio (b/a). Distances were calculated for all melanosome types at each wavelength and subsequently used to determine the average photoemission current of the shadows from which the absorption coefficients were calculated.

The path length of the experiments were calculated from an average of the different chord lengths through the ellipsoidal melanosomes that corresponded to points in the observed

shadows. We have previously demonstrated[20] that the average path length, l, through the ellipsoidal melanosomes is calculated through the following equation:

$$l = \frac{\int_{\chi}^{c}\int_{-\tau}^{\tau} 2\{b^2 - [(b^2x^2)/a^2] - [(b^2z^2)/c^2]\}^{1/2}\,dx\,dz}{\int_{\chi}^{c}\int_{-\tau}^{\tau} dx\,dz} \tag{3}$$

Here, a and b are the equatorial radii along the x and y axes, respectively, c is the polar radius along the z axis, and $\tau = [a^2 - (a^2z^2)/c^2]^{1/2}$. The polar distance, χ, which is obtained directly from the PEEM images, accounts for portions of the shadow regions that map onto chord lengths that extend below the center of the melanosome. In this analysis, the ellipsoidal melanosomes were assumed to be oriented perpendicular to the direction of incident light, which is reasonable with small aspect ratios that approach a spherical shape. However, for melanosomes with an aspect ratio that was large enough to determine the exact orientation in the PEEM image, it was necessary to take into account the angle between the incident light and the long axis of the melanosome. As previously described,[21] the average path length for a rotated ellipsoidal melanosome is

$$l = \frac{\int_{\chi}^{c}\int_{-\tau_2}^{\tau_2} s(X,z,\theta)\,dx\,dz}{\int_{\chi}^{c}\int_{-\tau_2}^{\tau_2} dx\,dz} \tag{4}$$

where

$$\begin{aligned} s(X,z,\theta) = 2\{[a^2b^2[-c^2X^2\cos(\theta)^4 \\ + \cos(\theta)^2[a^2(c^2 - z^2) - 2c^2X^2\sin(\theta)^2] \\ - \sin(\theta)^2[b^2(-c^2 + z^2) \\ + c^2X^2\sin(\theta)^2]]]/[c^2[a^2\cos(\theta)^2 + b^2\sin(\theta)^2]^2]\}^{1/2} \end{aligned}$$

and

$$\begin{aligned} \tau_2 = \{[(c^2 - z^2)[a^2\cos(\theta)^2 \\ + b^2\sin(\theta)^2]]/c^2\}^{1/2}/\{[\cos(2\theta)]^2\}^{1/2} \end{aligned}$$

The above analysis is accurate for melanosomes that are rotated in a counterclockwise rotation around the z axis by θ radians.

RESULTS

PEEM images of a single adult bovine RPE melanosome are shown in Figure 1 for each wavelength examined. In each image, a shadow was visualized behind the melanosome; the direction of the incident light is represented by the white arrow at the left bottom of panel a and is the same for all images. The melanosomes themselves are not observed in the PEEM images generated with wavelengths greater than ~270−280 nm as the photoionization threshold potential of eumelanin is ~4.5 ± 0.2 eV (276 nm).[27] The substrate, however, is photoionized at all wavelengths examined and thus the generated shadows were visualized throughout the experiment. The images shown in Figure 1 are representative of the wavelength-dependent PEEM images obtained for each of the studied melanosomes.

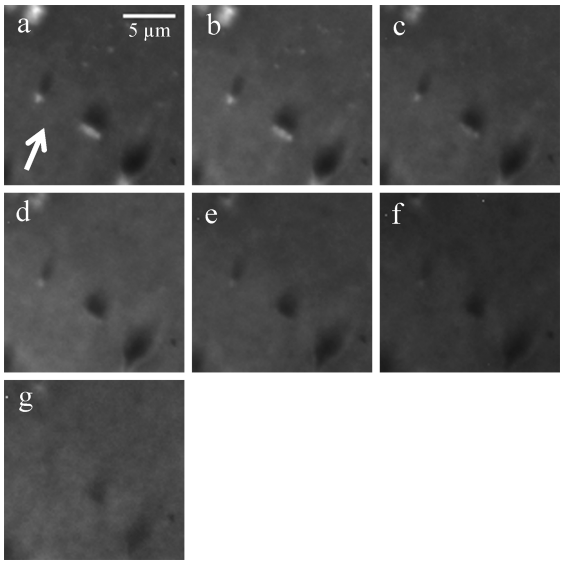

Figure 1. A sequence of PEEM images showing the wavelength-dependence of a single adult bovine RPE melanosome and its shadow on a SiC substrate. Images a−g were obtained upon illumination with laser wavelengths 244, 257, 270, 280, 290, 300, and 310 nm, respectively. The white arrow drawn in the bottom left of panel a represents the direction of incident light on the sample.

As described in the experimental methods, the absorption coefficient, εc, measurements required using a tunable pulsed laser source and SiC substrates so that the shadow could be visualized over the wavelength region examined. Furthermore, as a result of the low-pulsed energy of the laser and a desire to ensure a large spatial sampling, a field of view of 150 μm was required for the images. These experimental details are different than those where images were collected at λ = 244 nm using a Ar^+ ion CW laser on Ti at a 50 μm field of view.[21] Because of the signal intensity needed to resolve differences between the shadow and the substrate, using Ti would restrict the collection of the absorption spectra to wavelengths higher in energy than ~285 nm as its work function is 4.33 eV (287 nm). As shown in the bar chart in Figure 2, there are differences between the calculated absorption coefficients when measured on different substrates, at differing magnifications and using CW and pulsed laser sources. However, it is important to note there is no systematic variation when comparing the different experimental approaches. The calculated wavelength-dependent absorption coefficients reported herein are all obtained under identical experimental conditions and thus, relative values between samples and the wavelength dependence of the absorption coefficient arise from changes in the absorption properties of the melanosomes, not instrumental sources.

The measured εc at λ = 244 and 300 nm are listed in Table 1 along with the previously reported[8,21] DHICA:DHI ratios for the bovine eye melanosomes. The reported εc values are a result of an average of the full data set collected for each type of melanosome examined. Variability in εc was observed between individual melanosomes isolated from each tissue, but as previously discussed in detail,[20−22] this results from the fact that the path length used in calculating εc is set to the most probable value (determined from a size-analysis using scanning electron microscopy (SEM) images). As an example, SEM analysis of choroid shows these melanosomes to be ellipsoidal with dimensions

Table 1. Measured εc Values at λ = 244 and 300 nm as Compared to the Previously Reported[8,21] DHICA:DHI Ratios for Melanosomes Isolated from Bovine Eye Tissues

type	age	DHICA:DHI	εc^* (244 nm)/cm^{-1}	εc^* (300 nm)/cm^{-1}
RPE	newborn	1.30:1	4970 (1260)	2865 (730)
	adult	0.80:1	5100 (1675)	3495 (1145)
choroid	newborn	2.32:1	3175 (625)	1720 (340)
	adult	1.00:1	4495 (765)	1935 (330)
iris	adult	0.26:1	3270 (695)	1780 (380)

* The error in the calculated value of εc for the set of melanosomes examined is given in parentheses.

of 860 ± 120 and 630 ± 90, for the long and short axis, respectively.[8] The width of the distribution represents the FWHM. The reason this is done is because of the limited spatial resolution of the PEEM,[28] which for ellipsoidal objects is ~30−50 nm. This is further compounded by the fact that only a portion of the melanosome is revealed in the PEEM image because the light is incident on the sample at an angle of 13° from the plane of the surface. This means that the distribution in the lengths of the axes of the melanosomes is on the order of the PEEM resolution, and hence the PEEM image itself cannot be used to determine the melanosome dimensions directly. Thus, the error reported in Table 1 for the averaged εc arises from setting the path length of all melanosomes to the most probable value. The absorption coefficient depends linearly on the path length, and since the size distribution is symmetric around the most probable value, we would expect to observe variation among individual melanosomes, but the average value should reflect that intrinsic to the particular melanosome being examined.

The averaged εc values for choroid, iris and RPE melanosomes are plotted as a function of wavelength in Figure 3. The data shown are for melanosomes isolated from adult samples; newborn melanosomes show similar trends. Generally, εc values decreased with increasing wavelength, as expected from previous measurements reported[6,14,15,29,30] on synthetic model melanins. Furthermore, as evidenced in Figure 3, the absorption coefficients of bovine RPE melanosomes is on average about 1.5-fold greater than those for melanosomes isolated from bovine choroid or iris tissues, regardless of age. In addition, the iris melanosomes exhibit an absorption feature around 270 nm, and both iris and RPE melanosomes exhibit a feature around 300 nm.

DISCUSSION

The attenuation of incident light by a melanosome occurs through two processes, absorption and scattering. Because of the relative size of the melanosome and the wavelength of UV light, scattering effects must be considered. Although it is difficult to evaluate the contribution of scattering and absorption to signals observed on bulk samples, the two effects can be disaggregated within the shadow region of a single melanosome in the PEEM images. As previously discussed,[20] the portion of the shadow region that is void of significant scattering contributions was determined following the methodology outlined by Chelaru et al.[26] Briefly, diffraction will influence the intensity in the shadow region beginning at a distance from the melanosome corresponding to the first maximum in the diffraction pattern observed on the substrate. This distance can be calculated from the Fraunhofer diffraction pattern of an elliptical aperture of the same dimensions as the melanosomes as the two diffraction patterns are the same except for an inversion of the intensity distributions. This calculation, outlined in the experimental methods section (eq 2), was used for each melanosome at all wavelengths. As long as the region of the shadow analyzed is determined in this manner, it is the case that the calculated εc values for the melanosomes reflect absorption.

It is important to also acknowledge that although melanosomes are mainly comprised of eumelanin, they also contain proteins, lipids and various ions. While most lipids and amino acids exhibit negligible absorption between λ = 244 − 310 nm, the aromatic amino acids do absorb in this spectral range. The absorption maxima (extinction coefficient) of the aromatic amino acids Phe, Tyr, and Trp are 257.4 nm (165 M^{-1} cm^{-1}), 274.6 nm (1430 M^{-1} cm^{-1}), and 279.8 nm (6000 M^{-1} cm^{-1}), respectively,[31] with the extinction coefficients of the latter two on the order of the observed εc values. The contribution of the protein to the absorption measurements can be deduced from reported amino acid profiles of melanosomes. The protein content of the studied melanosomes increases from RPE to iris to choroid and ranges from 9−15%.[8] The distributions of the amino acids, however, are similar and the aromatic amino acid content makes up less than 10% of the protein composition for each type of melanosome.[8] Therefore, the contribution of the aromatic amino acids is expected to be at most 1.5% of the total absorption throughout the spectral range studied, which is negligible. Therefore the measured absorption predominately reflects that of the eumelanin pigment and as a result Figure 3 represents quantitative absorption spectra of the pigment contained within bovine RPE, choroid and iris melanosomes.

Eumelanin is built from varying amounts of the monomeric dihydroxyindole building blocks, DHI and DHICA (Table 1).[8] As discussed above, initial single-wavelength PEEM experiments[21] on intact melanosomes (measured with the experimental conditions reported as "A" in Figure 2) at λ = 244 nm suggested εc of the melanosome increases with increasing DHICA:DHI ratios. This conclusion was obtained by postulating that the absorption would scale linearly with the relative content of DHI and DHICA, in which case, we would predict

$$A = l(\varepsilon c)_{\text{eumelanin}} = l(\varepsilon_{\text{DHI}}[\text{DHI}] + \varepsilon_{\text{DHICA}}[\text{DHICA}]) \quad (5)$$

In terms of mole fraction, X, eq 5 becomes

$$\varepsilon_{\text{eumelanin}} = \varepsilon_{\text{DHI}} X_{\text{DHI}} + \varepsilon_{\text{DHICA}} X_{\text{DHICA}} \quad (6)$$

Since the total mole fraction is unity, $1 - X_{\text{DHICA}} = X_{\text{DHI}}$, eq 6 can be simplified to

$$\varepsilon_{\text{eumelanin}} = X_{\text{DHICA}}(\varepsilon_{\text{DHICA}} - \varepsilon_{\text{DHI}}) + \varepsilon_{\text{DHI}} \quad (7)$$

Literature values for the extinction coefficients of DHI and DHICA reveal that they are somewhat sensitive to experimental conditions, such as pH.[32−37] Taking an average of the reported values gives 2610 and 5530 M^{-1} cm^{-1} at λ = 244 nm, for DHI and DHICA, respectively. Figure 4 shows this original data, the εc value determined for melanosomes on a Ti substrate using CW Ar^+ ion laser at λ = 244 nm, plotted as a function of the mole fraction of DHICA contained in the melanosomes. The solid line in the plot, is drawn between the average ε values of the two monomers (2610 and 5530 M^{-1} cm^{-1}), and therefore represents the predicted absorption coefficients, eqs 5−7. We

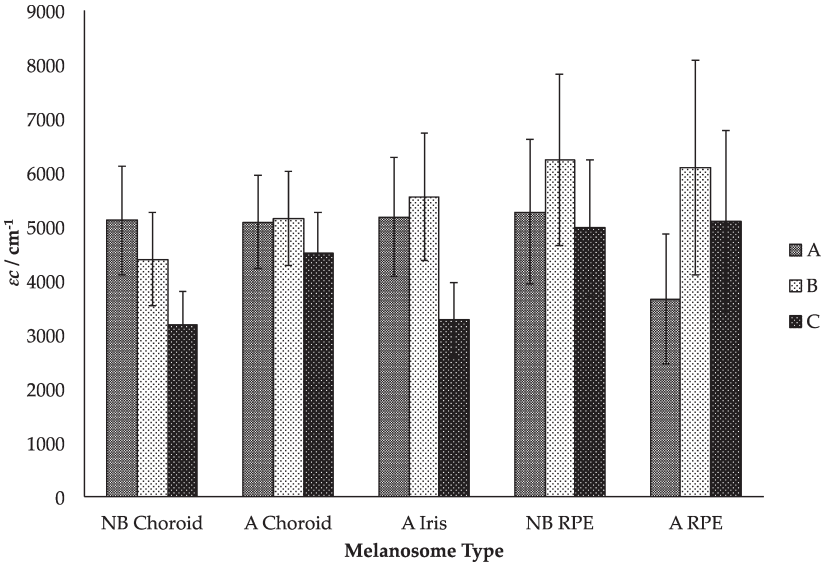

Figure 2. Average εc values as measured at $\lambda = 244$ nm with (A) 50 μm field of view (FOV), Ar^+ ion CW laser and Ti substrate, (B) 150 μm FOV, Ar^+ ion CW laser and SiC substrate, and (C) 150 μm FOV, pulsed nanosecond laser and SiC substrate.

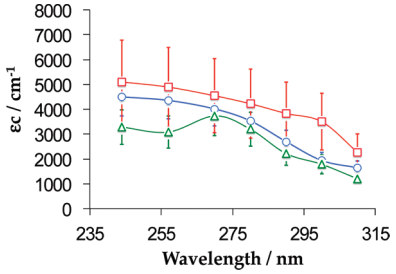

Figure 3. Summary of the average measured absorption coefficients of the bovine melanosomes versus wavelength; (□) RPE, (○) choroid, and (△) iris.

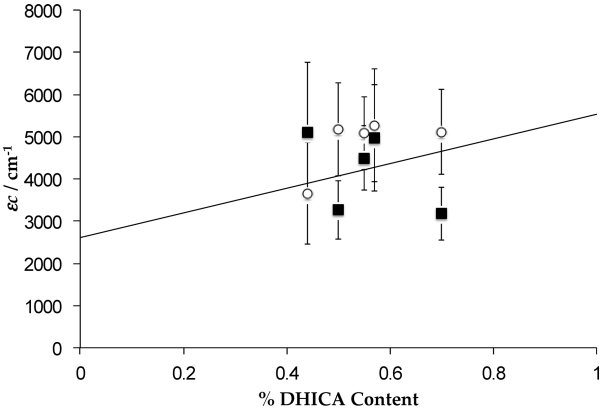

Figure 4. Plot of the observed absorption coefficient versus DHICA content at $\lambda = 244$ nm. The open circles were obtained using a Ti substrate, the 244-nm output from an intracavity doubled Ar^+ ion laser and a field of view of 50 μm. The dark squares were obtained using a SiC substrate, 244-nm from a pulsed nanosecond laser and a field of view of 150 μm. The line is representative of the predicted absorption as arising from the sum of the absorption of contributing DHI and DHICA monomers.

previously concluded[21] from this plot that the observed εc values are consistent with that predicted by eq 7, and suggested then that the absorption of natural melanins can be quantified in terms of relative content of the two constituent monomers, weighted by their relative mole fractions. However, the region probed (% DHICA 0.4−0.7) and the spread of the data certainly indicate that this conclusion requires further testing to be established and generalized. In fact, this conclusion is challenged by the εc values measured with SiC substrates and a tunable pulsed nanosecond laser (also shown in Figure 4). While one could attribute the lack of correlation to the precision of the PEEM technique, and the assumption of path length in particular, it is more reasonable to conclude that εc does not scale in accordance with eq 5 and that the region of DHICA content probed experimentally in Figure 4 is too narrow to make the conclusion about how the system behaves as a function of DHICA:DHI content. Unfortunately, this is the range associated with the ocular melanosomes and so we cannot obtain data on comparable systems at any arbitrary composition.

The lack of an additive relationship between εc and monomer content is more evident in the longer UV wavelength region of the spectrum. The shapes of the absorption spectra of DHI[34] and DHICA[35] are similar in the spectral region from 240 to 270 nm, but differ significantly in shape in the UV-A with the absorption maxima (extinction coefficient) being $\lambda = 296$ nm ($3310\ M^{-1}\ cm^{-1}$) and $\lambda = 320$ nm ($14\,000-16\,000\ M^{-1}\ cm^{-1}$), respectively. If we were to model the wavelength-dependent absorption of the melanosomes as described in eq 7, we would obtain absorption spectra similar to Figure 5A, where the DHICA extinction coefficient increases the absorption at wavelengths nearing the UV-A. The measured absorption spectra presented in Figure 3, however, are in stark contrast to those predicted. A decrease in the absorption is observed in the longer wavelength regions. Furthermore, as shown in Figure 5B, a plot of the melanosome absorption coefficients at $\lambda = 300$ nm as a function of the percentage of DHICA content reveals a decrease in εc with an increase of DHICA content. The observed trend does not extrapolate to the limiting values of the DHI and DHICA extinction coefficients clearly showing that the absorption

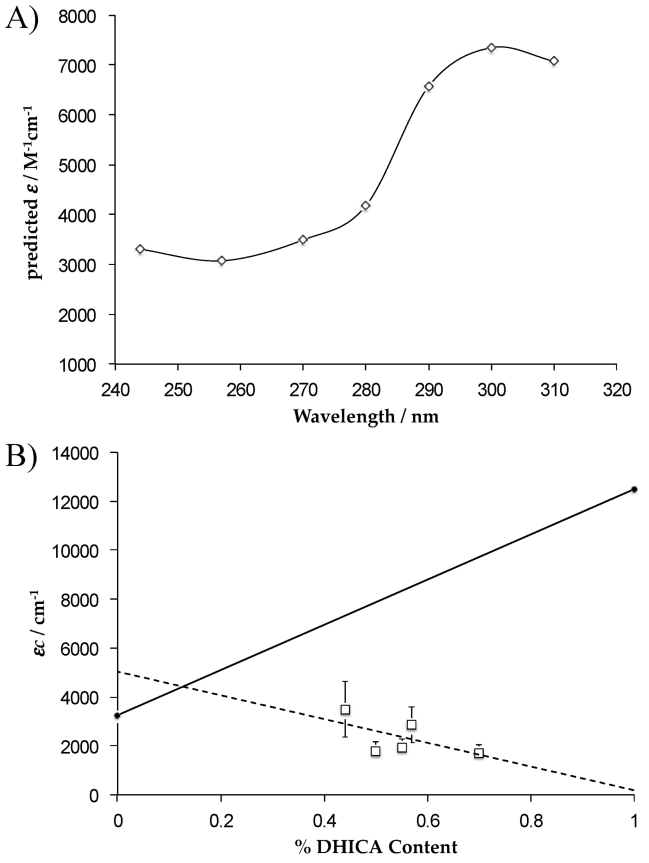

Figure 5. (A) Predicted absorption spectrum based on the determined monomer composition for adult bovine RPE melanosomes (0.44 DHICA content). (B) Plot of the observed εc versus DHICA content at λ = 300 nm (open squares). The data points at 0 and 1% DHICA are representative of the averaged DHI and DHICA extinction coefficients at this wavelength. The solid line drawn between the points is the predicted absorption as arising from the sum of the absorption of contributing DHI and DHICA monomers. The observed trend (dashed line) is in stark contrast to this prediction.

properties of melanosomes are not related to those of the constituent DHI and DHICA monomers. The same behavior is observed throughout the λ = 280−310 nm region.

Despite extensive experimental studies conducted on synthetic and natural eumelanin, including its soluble fraction, the structures of the natural oligomers formed from DHI and DHICA have evaded characterization. As a result, a thorough understanding of the unique optical properties of eumelanins has remained an immensely complex topic. The absorption data of intact, natural melanosomes offers a direct view into the oligomeric structure of the eumelanin pigment. As has been discussed, the natural oligomeric structure is not reflective of the electronic structure of the monomers throughout the ultraviolet. This is most notable in the UV-A region where the low energy band of DHICA appears to have a negligible effect on the absorption of the pigment. These results indicate that polymerization of DHICA into the melanin pigment disrupts the electronic structure of these monomeric building blocks; that polymerization modifies the electronic structure of the monomers in the resulting oligomer. Recently, papers[35,36,38−40] have been published that provide insight into UV−visible absorption properties of the evolution of the DHI and DHICA monomers into larger

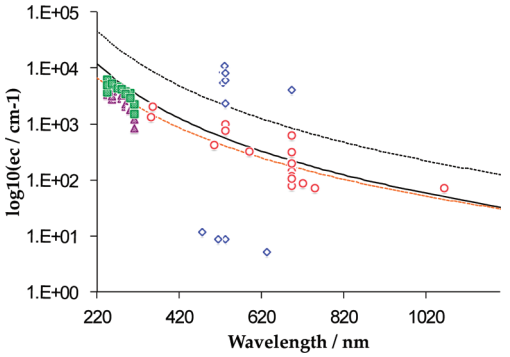

Figure 6. Comparison of the absorption coefficients measured for uveal (iris and choroid) and RPE melanosomes (shaded triangle and square data points, respectively) with previously reported cutaneous[14,15] (open circle) and RPE[15−19,30,41] (open diamond) melanosome absorption coefficients and previously predicted[15] cutaneous (solid line) and RPE (short dashed line) spectra. The lowest curve shown (long dashed line) is the best fit of the functional form $\varepsilon c = A\lambda^{-B}$ to the complete data set, $\varepsilon c(\lambda_{nm}) = 1.76 \times 10^{11}\ \lambda^{-3.17}\ cm^{-1}$. The middle and top curves are the corresponding functions reported by Jacques and co-workers for cutaneous and RPE melanosomes, the exponent in each of those curves being −3.48, similar to that found for the entire data set.

oligomeric structures (dimer to tetramer). The collective work observes absorption spectral shapes of the DHI and DHICA monomers that gradually shift toward the broadband eumelanin spectrum upon oxidative polymerization. Meredith and co-workers have examined the oligomerization of DHICA.[35,40] In a time-dependent study of DHICA oligomerization, in NaOH solutions, the absorption maximum at λ = 320 nm was found to decrease as a function of time, a 20% hyperchromism was observed for this band for the DHICA oliogmer compared to that of the monomer, and the absorption in the region from 240 to 300 nm increased. This then leads to a "flattening" of the absorption spectrum in the UV region, consistent with the behavior observed for the intact melanosomes in this study. Density functional theory calculations reveal the HOMO−LUMO gap decreases with oligomerization, providing an explanation for the red-shift in the near-UV absorption band that accompanies oligomerization.[35] Different chemical linkages between the monomers affect the spectroscopic properties differently, and Meredith and co-workers attribute the optical spectrum to reflect the superposition of the absorbance properties of a distribution of oligomers. Specifically, with an increasing number of inter-monomer bonds, the absorption spectrum undergoes a larger red-shift; this reflects the dependence of the degree of electron delocalization across the molecular framework on the linkages between monomers. While the relevance of these model oligerization studies and calculations to the actual eumelanin pigment remain to be assessed, these studies are consistent with the general features of the absorption spectra of the natural melanosomes presented herein.

Finally, we discuss these data in the context of reported values for εc of various types of melanosomes and the generalized expression for $\varepsilon c(\lambda_{nm})$ proposed by Jacques et al.[14,15] Figure 6 plots the absorption coefficients determined herein for RPE and uveal melanosomes along with previously reported values of the absorption coefficients of cutaneous[14,15] and RPE[15−19,30,41] melanosomes the visible region. In addition, the two wavelength-dependent curves predicted by Jacques et al.[14,15] for the

absorption coefficients of cutaneous and RPE melanosome are shown. At the midvisible wavelengths, the absorption coefficients of the RPE melanosomes are predominately larger than those for the cutaneous melanosomes. As seen, however, there is a large variance in the reported absorption coefficients; the values for RPE and cutaneous melanin ranged from 5 to 11 000 cm^{-1} and 78 to 997 cm^{-1} at the midvisible wavelengths, respectively. The large variance likely reflects differences in sample isolation and preparation, experimental methodology and perhaps, to a lesser degree, variation among the specimens used.[5,30,42] Our values of the UV-absorption data of uveal and RPE melanosomes all fall below the curve predicted for cutaneous melanosomes, and significantly below that predicted for RPE melanosomes. If we were to fit all of the data to a functional form similar to that presented[14,15] by Jacques, we would predict $\varepsilon c(\lambda_{nm}) = 1.76 \times 10^{11}\ \lambda^{-3.17}\ cm^{-1}$. Note, Jacques' prediction was based on the scaling of the in vivo spectrophotometer measurements of the cutaneous melanin to the average cutaneous absorption coefficient measured at $\lambda = 694$ nm.[14] The updated prediction is based on a functional fit of all the data.

Although to a lesser extent, similar to Jacques, we find that the absorption coefficients for bovine RPE melanosomes are, on average, greater than those measured for the uveal melanosomes. That result could still suggest that either the eumelanin pigment is present in greater density or that there is an underlying difference in the eumelanic molecular structure. This could also be a reflection of the fact that RPE melanosomes have a different embryonic origin than the uveal melanosomes. We further find that comparison of these spectra across the UV region reveal that the iris melanosomes exhibits a unique absorption feature ~270 nm, and both iris and RPE melanosomes exhibit a feature around ~300 nm. The origin of the spectral features remains unknown, but could be a reflection of a different structure of the constituent melanin. The iris melanosome contains the least amount of DHICA among the samples studied (Table 1), and it is possible the ~270 nm absorption is characteristic of a pigment that is predominantly comprised of DHI.

The differences between the choroid and iris melanosome absorption spectrum indicates that the absorption properties are not simply linked to their embryonic origin. It is possible, however, that the feature at ~300 nm present in the spectrum for iris melanosomes arises from imperfect separation of iris stroma and iris pigment epithelial cells. The latter also contain melanosomes, and share the same embryonic origin of RPE cells. While great care was taken in isolating these samples, it is difficult to ensure that only the uveal melanosomes are present in samples collected through dissection, and so it may be that the feature at ~300 nm is unique to melanosomes in pigment epithelial cells.

CONCLUSIONS

The absorption coefficients of natural intact melanosomes from bovine eye tissues have been directly quantified. The lower-energy UV-A region provides support that the electronic structure of the naturally occurring eumelanic oligomers do not reflect the electronic structure of the monomers. The currently available wavelength-dependent absorption data on melanosomes from 1020 to 240 nm can be well described by a single function of the form: $\varepsilon c(\lambda_{nm}) = 1.76 \times 10^{11}\ \lambda^{-3.17}\ cm^{-1}$. The absorption coefficients of the RPE melanosomes are ~1.5 larger than those of uveal melanosomes, suggesting that these organelles, of different embryonic origin may have different pigment densities or differences in the structure of their constituent eumelanin.

AUTHOR INFORMATION

Corresponding Author

*E-mail: john.simon@virginia.edu.

ACKNOWLEDGMENT

This research was supported by Duke University. D.N.P. is grateful for the support of the Charles Bradsher and William Krigbaum Fellowships. We thank Dr. Lian Hong for the sample isolation and size analysis data and Profs. Shosuke Ito and Kazumasa Wakamatsu for the chemical degradation analyses of the melanosomes. We thank Dr. Tong-Ho Kim and Prof. April Brown for helpful assistance and discussions concerning SiC wafers. We also thank Prof. Robert J. Nemanich for use of the photoemission electron microscope and the UV argon ion laser.

REFERENCES

(1) Ito, S.; Wakamatsu, K. *Photochem. Photobiol.* **2008**, *84*, 582–592.
(2) Tsukamoto, K.; Palumbo, A.; d'Ischia, M.; Hearing, V. J.; Prota, G. *Biochem. J.* **1992**, *286*, 491–495.
(3) Ito, S. *Biochim. Biophys. Acta* **1986**, *883*, 155–161.
(4) Kollias, N.; Sayre, R. M.; Zeise, L.; Chedekel, M. R. *J. Photochem. Photobiol. B: Biol.* **1991**, *9*, 135–160.
(5) Sarna, T. *J. Photochem. Photobiol. B-Biol.* **1992**, *12*, 215–258.
(6) Meredith, P.; Sarna, T. *Pigment Cell Res.* **2006**, *19*, 572–594.
(7) Dryja, T. P.; Oneildryja, M.; Albert, D. M. *Invest. Ophthalmol. Vis. Sci.* **1979**, *18*, 231–236.
(8) Liu, Y.; Hong, L.; Wakamatsu, K.; Ito, S.; Adhyaru, B. B.; Cheng, C.-Y.; Bowers, C. R.; Simon, J. D. *Photochem. Photobiol.* **2005**, *81*, 510–516.
(9) Hu, D.-N.; Wakamatsu, K.; Ito, S.; Mccormick, S. A. *Melanoma Res.* **2009**, *19*, 75–79.
(10) Nordlund, J. J. *J. Geriatr. Dermatol.* **1989**, *5*, 91–108.
(11) Schraermeyer, U.; Heimann, K. *Pigment Cell Res.* **1999**, *12*, 219–236.
(12) Bumsted, K. M.; Barnstable, J. C. *Invest. Ophthalmaol. Vis. Sci.* **2000**, *41*, 903–908.
(13) Boissy, R. E.; Hornyak, T. J. In *The Pigmentary System: Physiology and Pathology*; 2nd ed.; Norlund, J. J., Boissy, R. E., Hearing, V. J., King, R. A., Oetting, W. S., Ortonne, J.-P., Eds.; Blackwell Publishing: Malden, 2006; pp 91−107.
(14) Jacques, S. L.; McAuliffe, D. J. *Photochem. Photobiol.* **1991**, *53*, 769–775.
(15) Jacques, S.; Glickman, R.; Schwartz, J. *Proc. SPIE* **1996**, *2681*, 468–477.
(16) Strauss, M.; Amendt, P. A.; London, R. A.; Maitland, D. J.; Glinsky, M. E.; Lin, C. P.; Kelly, M. W. *Proc. SPIE* **1997**, *2975*, 261–270.
(17) Brinkmann, R.; Huttmann, G.; Rogener, J.; Roider, J.; Birngruber, R.; Lin, C. P. *Lasers Surg. Med.* **2000**, *27*, 451–464.
(18) Glickman, R.; Jacques, S.; Hall, R.; Kumar, N. *Proc. SPIE* **2001**, *4257*, 134–141.
(19) Neumann, J.; Brinkmann, R. *J. Biomed. Opt.* **2005**, *10*, 024001.
(20) Peles, D. N.; Simon, J. D. *J. Phys. Chem. B* **2010**, *114*, 9677–9683.
(21) Peles, D. N.; Lin, E.; Wakamatsu, K.; Ito, S.; Simon, J. D. *J. Phys. Chem. Lett.* **2010**, *1*, 2391–2395.
(22) Peles, D. N.; Simon, J. D. *Photochem. Photobiol.* **2010**, *86*, 279–281.
(23) Ade, H.; Yang, W.-C.; English, S. L.; Hartman, J.; Davis, R. F.; Nemanich, R. J.; Litvinenko, V. N.; Pinayev, I. V.; Wu, Y.; Madey, J. M. J. *Surf. Rev. Lett.* **1998**, *5*, 1257–1268.
(24) Buckanie, N. M.; Göhre, J.; Zhou, P.; von der Linde, D.; Horn-Von Hoegen, M.; Meyer Zu Heringdorf, F.-J. *J. Phys.: Condens. Matter* **2009**, *21*, 314003.

(25) Glickman, R. D.; Jacques, S. L.; Schwartz, J. A.; Rodriguez, T.; Lam, K.-W.; Buhr, G. *Proc. SPIE* **1996**, *2681*, 460–467.
(26) Chelaru, L. I.; Hoegen, M. H.-V.; Thien, D.; Heringdorf, F.-J. M. *Phys. Rev. B* **2006**, *73*, 115416.
(27) Garguilo, J.; Hong, L.; Edwards, G. S.; Nemanich, R. J.; Simon, J. D. *Photochem. Photobiol.* **2007**, *83*, 692–697.
(28) Peles, D. N.; Simon, J. D. *Photochem. Photobiol.* **2009**, *85*, 8–20.
(29) Sarna, T.; Sealy, R. C. *Photochem. Photobiol.* **1984**, *39*, 69–74.
(30) Sardar, D. K.; Mayo, M. L.; Glickman, R. D. *J. Biomed. Opt.* **2001**, *6*, 404–410.
(31) Wetlaufer, D. *Adv. Protein Chem.* **1962**, *17*, 303–390.
(32) Benigni, J. D.; Minnis, R. *J. Hetero. Chem.* **1965**, *2*, 387–392.
(33) Ito, S.; Nicol, J. A. C. *Biochem. J.* **1974**, *143*, 207–217.
(34) Murphy, B. P.; Schlutz, T. M. *J. Org. Chem.* **1985**, *50*, 2790–2791.
(35) Tran, M.; Powell, B.; Meredith, P. *Biophys. J.* **2006**, *90*, 743–752.
(36) d'Ischia, M.; Crescenzi, O.; Pezzella, A.; Arzillo, M.; Panzella, L.; Napolitano, A.; Barone, V. *Photochem. Photobiol.* **2008**, *84*, 600–607.
(37) Gauden, M.; Pezzella, A.; Panzella, L.; Napolitano, A.; d'Ischia, M.; Sundström, V. *J. Phys. Chem. B* **2009**, *113*, 12575–12580.
(38) Pezzella, A.; Panzella, L.; Crescenzi, O.; Napolitano, A.; Navaratnam, S.; Edge, R.; Land, E. J.; Barone, V.; d'Ischia, M. *J. Org. Chem.* **2009**, *74*, 3727–3734.
(39) Pezzella, A.; Iadonisi, A.; Valerio, S.; Panzella, L.; Napolitano, A.; Adinolfi, M.; d'Ischia, M. *J. Am. Chem. Soc.* **2009**, *131*, 15270–15275.
(40) Riesz, J.; Gilmore, J.; Mckenzie, R.; Powell, B.; Pederson, M.; Meredith, P. *Phys. Rev. E* **2007**, *76*, 021915.
(41) Williams, M. A.; Pinto, L. H.; Gherson, J. *Invest. Ophthalmol. Visual Sci.* **1985**, *26*, 657–669.
(42) Riesz, J.; Gilmore, J.; Meredith, P. *Biophys. J.* **2006**, *90*, 4137–4144.